Available online at www.sciencedirect.com
SCIENCE DIRECT®
Journal of Nuclear Materials 336 (2005) 201–209
journal of nuclear materials
www.elsevier.com/locate/jnucmat

Displacement cross-sections for tantalum and tungsten irradiated with protons at energies up to 1 GeV

C.H.M. Broeders [a,*], A.Yu. Konobeyev [a,b]

[a] *Institut für Reaktorsicherheit, Forschungszentrum Karlsruhe GmbH, Postfach 3640, 76021 Karlsruhe, Germany*
[b] *Institute of Nuclear and Power Engineering, 249020 Obninsk, Russia*

Received 3 June 2004; accepted 21 September 2004

Abstract

The displacement cross-sections have been analyzed for tantalum and tungsten irradiated with protons at energies from several keV up to 1 GeV using different nuclear models and approaches to obtain the number of defects in irradiated material. The displacement cross-section for proton elastic scattering has been obtained using the data from ENDF/B-VI Proton Sublibrary and with the help of an optical model. The nonelastic displacement cross-section has been calculated by means of various nuclear models incorporated in the MCNPX code. The number of defects produced under high energy proton irradiation was calculated with the help of a combination of binary collision approximation and molecular dynamics models.

1. Introduction

The calculation of the displacement cross-sections for tantalum and tungsten is important for the evaluation of the radiation durability of these materials for use as solid target in the various concepts of the sub-critical accelerator driven systems.

Recently the determination of reliable proton displacement cross-sections for tantalum and tungsten has got special interest in the TRADE project [1]. The evaluation of the displacement cross-sections for these elements encounters certain difficulties. The measurements of the defect production rate for tantalum and tungsten [1–6] show noticeable differences with the NRT model [7] predictions. At the same time the calculations basing on the method of the molecular dynamics (MD) are not in good agreement with the experimental data for high-energy proton irradiation [8].

In the present work the different approaches used for the displacement cross-section calculation are compared and analyzed for the primary proton energy range up to 1 GeV. The displacement cross-section for the elastic channel is calculated using various modern optical potentials and ENDF/B-VI data. The MCNPX code [9] is used to determine the displacement cross-sections for the nonelastic proton–nucleus interactions. The number of defects produced by the primary knock-on atoms (PKA) in materials is calculated with the help of the NRT model and the binary collision approximation

* Corresponding author. Tel.: +49 7247 822484; fax: +49 7247 823718/3824.
E-mail address: cornelis.broeders@irs.fzk.de (C.H.M. Broeders).

0022-3115/$ - see front matter © 2004 Elsevier B.V. All rights reserved.
doi:10.1016/j.jnucmat.2004.09.015

model (BCA) using the results obtained by the MD method.

2. Calculations using the NRT model

This section concerns the calculation of displacement cross-sections based on the NRT model described in Refs. [7,10]. The displacement cross-section is calculated by the formula

$$\sigma_{\mathrm{d}}(E_{\mathrm{p}}) = \sum_i \int_{E_{\mathrm{d}}}^{T_i^{\max}} \frac{\mathrm{d}\sigma(E_{\mathrm{p}}, Z_{\mathrm{T}}, A_{\mathrm{T}}, Z_i, A_i)}{\mathrm{d}T_i} \times \nu(T_i, Z_{\mathrm{T}}, A_{\mathrm{T}}, Z_i, A_i)\,\mathrm{d}T_i, \quad (1)$$

where E_{p} is the incident proton energy; $\mathrm{d}\sigma/\mathrm{d}T_i$ is the cross-section of energy transfer to recoil atom; Z_i and A_i are the atomic number and the mass number of the recoil atom, correspondingly; Z_{T} and A_{T} are the same for the target material; $\nu(T_i)$ is the number of Frenkel pairs produced by PKA with the kinetic energy T_i; $T_i^{\max}$ is the maximal energy of the PKA spectrum; E_{d} is the effective threshold displacement energy; the summing is for all recoil atoms produced in the irradiation.

The number of defects produced by the PKA in material $\nu(T)$ is calculated according to the NRT approach [7] with the value of 'k' parameters defined according to Robinson [10]

$$\nu(T) = \eta(T)\frac{0.8}{2E_{\mathrm{d}}}T_{\mathrm{dam}}(T), \quad (2)$$

$$T_{\mathrm{dam}}(T) = \frac{T}{1 + k(3.4008\varepsilon^{1/6} + 0.40244\varepsilon^{3/4} + \varepsilon)},$$

$$k = \frac{32}{3\pi}\left(\frac{m_{\mathrm{e}}}{M_{\mathrm{T}}}\right)^{1/2}\frac{(A_i + A_{\mathrm{T}})^{3/2}Z_i^{2/3}Z_{\mathrm{T}}^{1/2}}{A_i^{3/2}(Z_i^{2/3} + Z_{\mathrm{T}}^{2/3})^{3/4}},$$

$$\varepsilon = [A_{\mathrm{T}}T/(A_i + A_{\mathrm{T}})]\,[a/(Z_i Z_{\mathrm{T}} e^2)],$$

$$a = a_0(9\pi^2/128)^{1/3}\left(Z_i^{2/3} + Z_{\mathrm{T}}^{2/3}\right)^{-1/2},$$

where η is the defect production efficiency [6,8]; m_{e} is the mass of an electron; M_{T} is the mass of the target atom; a_0 is the Bohr radius; 'e' is the electron charge; the kinetic energy T is taken in keV.

The defect production efficiency η (Eq. (2)) defines the ratio of the real number of single interstitial atom vacancy pairs produced in material to the number of defects calculated by the NRT approach. In this Section the η value is taken equal to unity. The effective threshold displacement energy E_{d} equal to 90 eV is used for the displacement cross-section calculation for tantalum and tungsten [6].

2.1. Elastic proton scattering

The displacement cross-section for the proton elastic scattering is calculated by

$$\sigma_{\mathrm{d,el}}(E_{\mathrm{p}}) = \int_{E_{\mathrm{d}}}^{T_{\max}} \frac{\mathrm{d}\sigma(E_{\mathrm{p}}, Z_{\mathrm{T}}, A_{\mathrm{T}})}{\mathrm{d}T}\nu(T, Z_{\mathrm{T}}, A_{\mathrm{T}})\,\mathrm{d}T. \quad (3)$$

Generally, the spectrum of PKA produced by the proton elastic scattering includes the contributions from the screened Coulomb scattering in the material, the nuclear scattering and their interference.

The nuclear scattering does not make a real contribution in the $\mathrm{d}\sigma/\mathrm{d}T$ spectrum of tantalum and tungsten for the initial proton energy below 5 MeV, and the recoil spectrum is formed mainly by the screened Coulomb scattering. The screening effect disappears with the increase of the primary proton energy, and the displacement cross-section $\sigma_{\mathrm{d,el}}$ at the energies above several MeV can be calculated with a high accuracy by the Rutherford formula for the recoil spectrum: $\mathrm{d}\sigma/\mathrm{d}T = \alpha \cdot \mathrm{d}T/T^2$, where α is a constant. The ratio of the elastic displacement cross-section for tantalum and tungsten isotopes calculated for the screened Coulomb field to the cross-section obtained by the Rutherford formula is equal to 0.943 for the primary proton energy equal to 1 MeV, 0.975 for the proton energy 5 MeV and 0.983 for the 10 MeV-protons. The displacement cross-section for screened Coulomb scattering was calculated in the present work with the help of the approach from Refs. [11,12].

The contribution of the nuclear scattering in the recoil spectrum $\mathrm{d}\sigma/\mathrm{d}T$ also increases with the increase of the primary proton energy. The contribution becomes appreciable for the $\sigma_{\mathrm{d,el}}$ calculation at energies above 10 MeV, where the screening effect is small. It allows applying the nuclear optical model for the elastic displacement cross-section calculations at the initial proton energies considered.

Fig. 1 shows the ratio of the elastic displacement cross-section calculated taking into account the Coulomb scattering, the nuclear scattering and their interference to the cross-section obtained for the recoil spectrum corresponding to the pure Coulomb scattering for ^{181}Ta and ^{184}W. The angular distribution for proton elastic scattering on ^{181}Ta was calculated with the help of the optical model using the optical potential from Ref. [16]. The angular distributions for ^{184}W were taken from ENDF/B-VI Proton Sublibrary (Release 7). One can see that the nuclear scattering has a significant influence on the calculated $\sigma_{\mathrm{d,el}}$ value at proton energies above 10 MeV.

The use of different modern optical potentials demonstrates a similar description of the experimental proton angular distribution and gives similar values of the elastic displacement cross-section. Fig. 2 shows the proton angular distributions for ^{181}Ta calculated using the

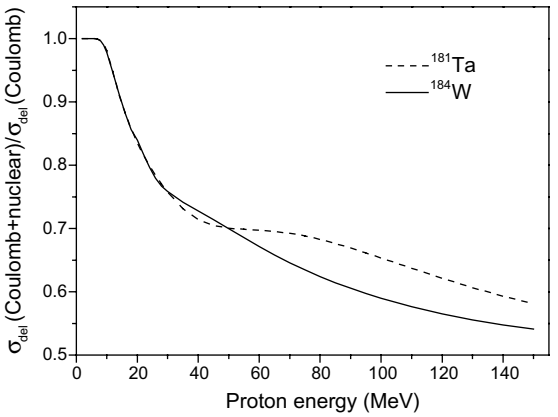

Fig. 1. The ratio of the elastic displacement cross-section calculated taking into account the Coulomb scattering, the nuclear scattering and their interference with the displacement cross-section obtained for the pure Coulomb scattering of ^{181}Ta and ^{184}W.

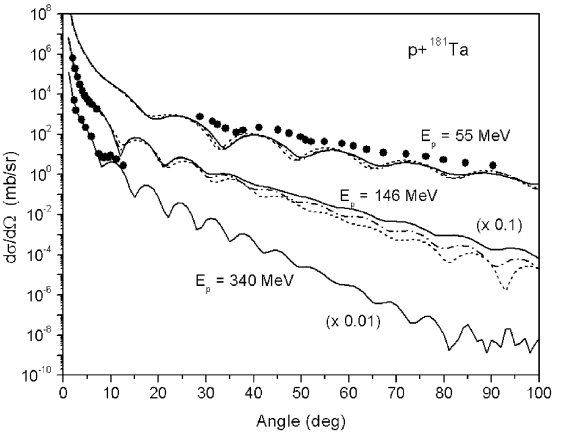

Fig. 2. The proton elastic angular distributions of ^{181}Ta calculated with the help of the optical potential from Ref. [13] (dash-dotted line), Ref. [14] (dash-double dotted line), Ref. [15] (solid line) and Ref. [16] (dashed line). The experimental data (cycles) are from Ref. [17] (55 MeV-protons), Ref. [18] (146 MeV) and Ref. [19] (340 MeV).

global optical potentials from Refs. [13–16] at different primary proton energies. The experimental data are from Refs. [17–19]. Good agreement is observed between the calculations and the measured data at the relatively small scattering angles for the initial proton energy 146 MeV and 340 MeV. The agreement for the 55 MeV-protons is worse and the different calculations give the similar result. Fig. 3 shows the $\sigma_{d,el}$ values for ^{184}W calculated with the help of the global optical potential from Ref. [13] at proton energies from 80 to 180 MeV, from Ref. [15] at 50–400 MeV and from Ref. [16] at the energies below 200 MeV. Fig. 3 shows also

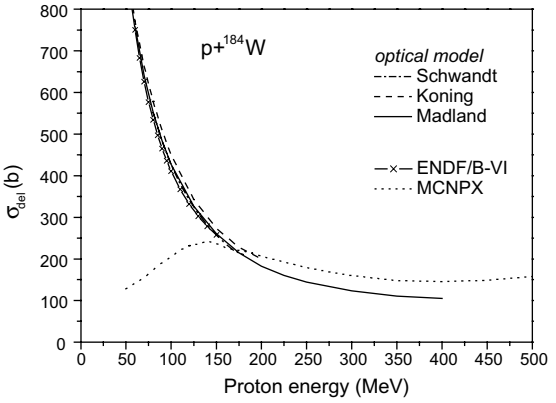

Fig. 3. The displacement cross-section of the proton elastic scattering calculated for ^{184}W using the optical potential from Ref. [13] (dash-dotted line), Ref. [15] (solid line), Ref. [16] (dashed line), the ENDF/B-VI data (solid cross line) and the MCNPX code [9] (dotted line).

the displacement cross-sections calculated using the evaluated proton elastic angular distributions from ENDF/B-VI at energies up to 150 MeV. There is good agreement between the $\sigma_{d,el}$ values obtained with the help of different optical potentials and the ENDF/B-VI data.

The displacement cross-section was calculated with the help of the MCNPX code [9] for comparison with the results of the optical model calculation. The PKA spectrum for elastic scattering has been evaluated from the standard output file 'histp' by the HTAPE3X code [20]. The calculated $\sigma_{d,el}$ values are shown in Fig. 3. One can see a certain difference between the results obtained using the ENDF/B-VI data, the optical model and the elastic scattering model incorporated in the MCNPX code. The reason of the discrepancy is not quite clear. Most likely the use of the 'proton elastic cross-section' in the MCNPX calculations ([20], p. 53) is based on a certain simplification in the description of the Coulomb scattering in the code. It could result in the discrepancy with an accurate optical model calculation. The same behavior of the displacement cross-section is observed in the LAHET code calculation [40,41].

2.2. Nonelastic proton interactions

The displacement cross-section for proton nonelastic interactions with target material $\sigma_{d,non}$ has been calculated with the help of the different models incorporated in the MCNPX code.

Fig. 4 shows the displacement cross-section $\sigma_{d,non}$ calculated with the help of the MCNPX code and the $\sigma_{d,non}$ values obtained using the recoil spectra from ENDF/B-VI for ^{184}W. The following intranuclear cascade evaporation models were used for the calculations [9]: Bertini/Dresner [21–23], ISABEL/Dresner [23–26],

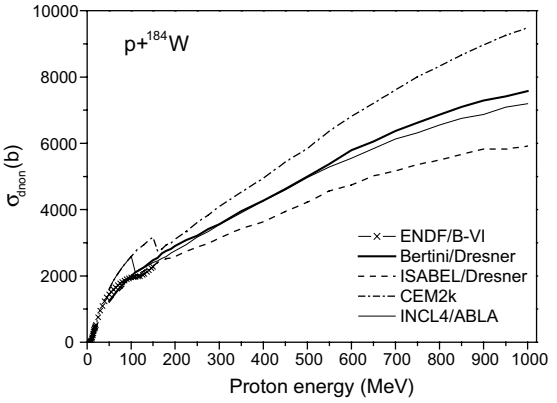

Fig. 4. The displacement cross-section of the proton nonelastic interactions with ^{184}W calculated using the ENDF/B-VI data (solid cross line) and the different nuclear models incorporated in the MCNPX code: Bertini/Dresner (solid thick line), ISABEL/Dresner (dashed line), CEM2k (dash-dotted line) and INCL4/ABLA (solid thin line).

CEM2k [27–31], INCL4/ABLA [32–35] with the default model parameters from Ref. [9]. The nonelastic displacement cross-section was calculated at energies from 50 MeV up to 1 GeV.

There is satisfactory agreement between the cross-sections obtained using the data from ENDF/B-VI below 150 MeV and the $\sigma_{d,non}$ values calculated with the help of the Bertini/Dresner and ISABEL/Dresner models. The $\sigma_{d,non}$ cross-sections calculated by the INCL4/ABLA and CEM2k have jumps near 100 MeV and 150 MeV. Good agreement is observed for the Bertini/Dresner and INCL4/ABLA calculations at energies from 100 MeV up to 1 GeV. The cross-sections calculated by the CEM2k model and by the ISABEL/Dresner model are noticeably different from the $\sigma_{d,non}$ values obtained with the help of the Bertini/Dresner and ICNCL4/ABLA models.

The observed difference in the calculated $\sigma_{d,non}$ values results from the different description of the particle emission spectra by the nuclear models considered. An example of such calculations is shown in Fig. 5 for the double differential cross-sections in the ^{181}Ta(p,p′) reaction. The experimental points are from Ref. [36].

Fig. 6 shows the integral recoil spectrum calculated with the help of the considered nuclear models for ^{184}W irradiated by 1 GeV-protons. The integral spectrum is the sum of the individual spectra for all nuclides produced in the nonelastic proton interactions with ^{184}W. The observed difference in the recoil spectra results in the scattering of the $\sigma_{d,non}$ values predicted by the different nuclear models. The most influence is due to the shape of the first peak in the $d\sigma/dT$ distribution (Fig. 6), which corresponds to the (p,xnyp) reactions. The fission peak does not play an important role due

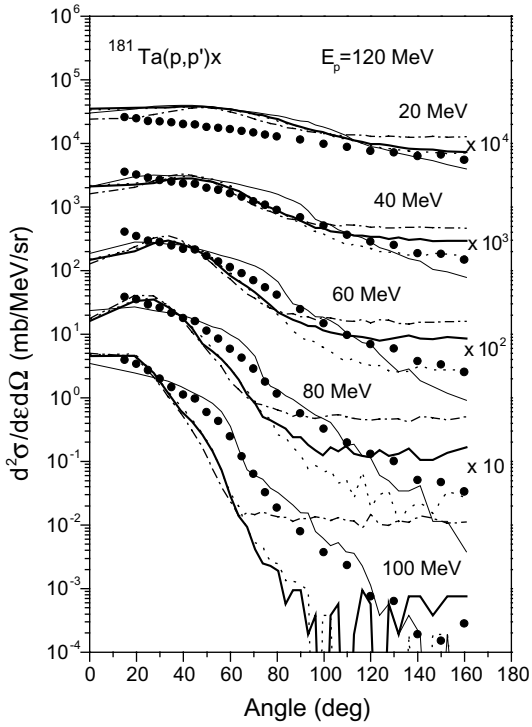

Fig. 5. The angular distributions of the ^{181}Ta(p,p′) reaction at 120 MeV primary proton energy and various proton emission energies calculated with the help of the different nuclear models incorporated in the MCNPX code and measured in Ref. [36]. See also captions in Fig. 4.

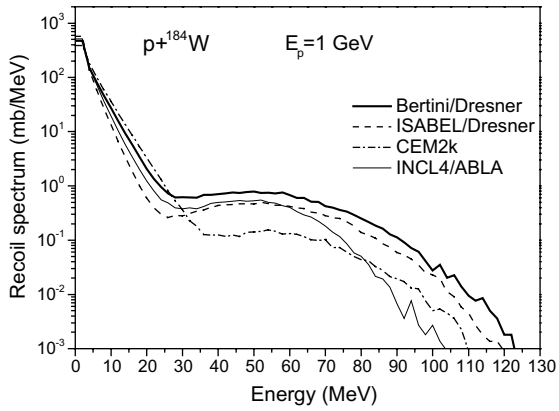

Fig. 6. The integral recoil spectrum of nonelastic 1 GeV-proton interactions with ^{184}W calculated with the help of the different nuclear models incorporated in the MCNPX code. See also captions in Fig. 4.

to the small contribution of the fission in the nonelastic proton cross-section (≈0.9% for 1 GeV), and in the nonelastic displacement cross-section (≈3.7%). The recoil spectra for ^{181}Ta and ^{184}W calculated by the Bertini/

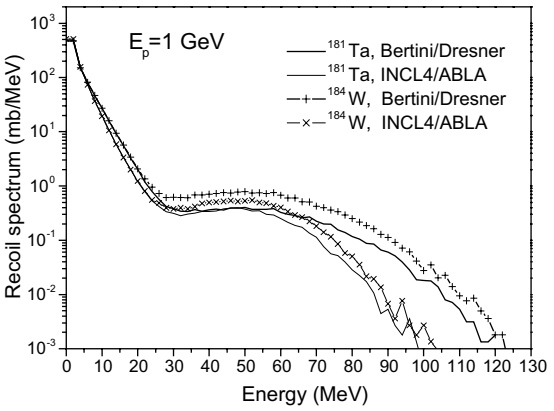

Fig. 7. The integral recoil spectrum of nonelastic 1 GeV-proton interactions calculated with the help of the Bertini/Dresner model for ^{181}Ta (solid thick line) and ^{184}W (crossed solid thick line), and with the help of the INCL4/ABLA model for ^{181}Ta (solid thin line) and for ^{184}W (crossed solid thin line).

Dresner model and the INCL4/ABLA model are compared in Fig. 7.

The observed uncertainty in the $\sigma_{d,non}$ values calculated using the different modern nuclear models (Fig. 4) cannot be overcame at present time. It should be considered as an error of the nonelastic displacement cross-section value obtained theoretically. This error is about 20–25%. Apparently, one should expect the same uncertainty for the calculations of the nonelastic displacement cross-sections at high energies performed for tungsten with the help of the other version of the MCNPX code [42] and the LAHET code [40].

2.3. Evaluation of the total displacement cross-section

The total value of the displacement cross-section was calculated as the sum of the proton elastic displacement cross-section $\sigma_{d,el}$ and the displacement cross-section for the proton nonelastic interactions $\sigma_{d,non}$.

The displacement cross-section for the proton elastic scattering has been calculated with the help of the optical model using the optical potentials from Refs. [15,16] at the initial proton energies from 5 MeV to 400 MeV. Below 5 MeV the $\sigma_{d,el}$ values were calculated using the differential scattering cross-section from Refs. [11,12]. The MCNPX code [9] has been used for the elastic displacement cross-section calculation at the energy from 400 MeV to 1 GeV. The values calculated were slightly fitted to the cross-sections obtained with the help of the Madland optical potential [15] at 400 MeV.

The nonelastic displacement cross-section has been calculated with the help of the Bertini/Dresner model and the MCNPX code. The recoil spectra from ENDF/B-VI were used to calculate the $\sigma_{d,non}$ values for tungsten isotopes with the mass number 182, 183, 184 and 186 at energies below 150 MeV. The evaluated total displacement cross-section is shown in Table 1 and in Fig. 8 for ^{181}Ta and a natural mixture of tungsten isotopes.

One should note that the displacement cross-section at keV energies is about two orders of magnitude higher than that at 1 GeV. This is due to the fact that the main mechanism of the energy loss in keV region for tantalum and tungsten is nuclear stopping. The electronic excitations with the increase of the primary ion energy result in a reduction of the energy retains for damage production.

3. Calculations using the BCA and MD models to obtain the number of defects produced in irradiated material

3.1. Tungsten

The number of defects produced by tungsten self-ion irradiation has been calculated by the MD method in Refs. [8,37]. The calculations have been performed at the energies below 100 keV. According to Ref. [8] the efficiency of the defect production η (Eq. (2)) is equal to unity at 1 keV and decreases with the energy growing up to ≈30 keV down to the value about 0.26.

The interaction of 1 GeV-protons with tungsten produces the recoil atoms with the kinetic energy considerably exceeding the maximal energy in the MD simulation [8,37]. To obtain the number of defects produced in material under the high energy proton irradiation the calculations were performed in the present work with the help of the BCA model basing on the results of the MD simulation from Ref. [8].

For an energetic ion moving in the material, the simulation of the atomic collision was performed with the help of the binary collision approximation model up to a certain 'critical' energy of the ion. Below this energy the BCA calculation was stopped and the number of defects has been calculated according to the result of the MD simulation [8] (Eq. (4a)). Such procedure was performed for all PKAs produced in the atomic collision cascade. The BCA calculations were carried out with the help of the IOTA code [38]. The value of the 'critical' energy should be taken as large as possible to minimize the effect of the overlapping of cascade branches before the MD simulation starts. In the present calculation the 'critical' energy was taken according to the high energy limit of the empirical equation [8] describing the efficiency of the defect production obtained from the MD calculation [8]. It corresponds to the damage energy T_{dam} equal to 31 keV and the defect production efficiency η equal to 0.26 [8]. For the case of the self-ion irradiation of tungsten this damage energy corresponds to the 'critical' energy of ions equal to 40.8 keV.

Table 1
Total proton displacement cross-sections evaluated for ^{181}Ta and ^{nat}W at energies up to 1 GeV

Proton energy (MeV)	Displacement cross-section (b)	
	^{181}Ta	^{nat}W
4.0×10^{-3}	0.0	0.0
4.1×10^{-3}	0.0	1.87
4.2×10^{-3}	2.30×10^{4}	7.27×10^{3}
4.3×10^{-3}	4.93×10^{4}	3.18×10^{4}
4.4×10^{-3}	7.37×10^{4}	5.69×10^{4}
4.5×10^{-3}	9.66×10^{4}	8.03×10^{4}
4.6×10^{-3}	1.18×10^{5}	1.02×10^{5}
4.7×10^{-3}	1.38×10^{5}	1.23×10^{5}
4.8×10^{-3}	1.56×10^{5}	1.42×10^{5}
5.0×10^{-3}	1.90×10^{5}	1.77×10^{5}
5.3×10^{-3}	2.33×10^{5}	2.21×10^{5}
5.6×10^{-3}	2.69×10^{5}	2.58×10^{5}
6.0×10^{-3}	3.07×10^{5}	2.97×10^{5}
8.0×10^{-3}	4.02×10^{5}	3.97×10^{5}
1.0×10^{-2}	4.30×10^{5}	4.27×10^{5}
1.2×10^{-2}	4.41×10^{5}	4.38×10^{5}
1.4×10^{-2}	4.42×10^{5}	4.40×10^{5}
1.6×10^{-2}	4.38×10^{5}	4.37×10^{5}
1.8×10^{-2}	4.32×10^{5}	4.31×10^{5}
2.0×10^{-2}	4.24×10^{5}	4.23×10^{5}
3.0×10^{-2}	3.79×10^{5}	3.80×10^{5}
5.0×10^{-2}	3.07×10^{5}	3.08×10^{5}
7.0×10^{-2}	2.58×10^{5}	2.59×10^{5}
0.10	2.10×10^{5}	2.11×10^{5}
0.15	1.63×10^{5}	1.64×10^{5}
0.20	1.34×10^{5}	1.35×10^{5}
0.30	1.00×10^{5}	1.01×10^{5}
0.40	8.10×10^{4}	8.17×10^{4}
0.50	6.84×10^{4}	6.89×10^{4}
0.70	5.26×10^{4}	5.31×10^{4}
1.0	3.95×10^{4}	3.99×10^{4}
1.5	2.84×10^{4}	2.86×10^{4}
2.0	2.23×10^{4}	2.25×10^{4}
3.0	1.58×10^{4}	1.60×10^{4}
4.0	1.24×10^{4}	1.25×10^{4}
5.0	1.02×10^{4}	1.03×10^{4}
7.0	7.66×10^{3}	7.74×10^{3}
10.0	5.53×10^{3}	5.59×10^{3}
15.0	3.84×10^{3}	3.87×10^{3}
20.0	3.05×10^{3}	3.08×10^{3}
30.0	2.53×10^{3}	2.55×10^{3}
40.0	2.41×10^{3}	2.41×10^{3}
50.0	2.37×10^{3}	2.37×10^{3}
60.0	2.34×10^{3}	2.34×10^{3}
80.0	2.36×10^{3}	2.35×10^{3}
100.0	2.38×10^{3}	2.36×10^{3}
120.0	2.35×10^{3}	2.33×10^{3}
150.0	2.57×10^{3}	2.54×10^{3}
200.0	3.00×10^{3}	3.05×10^{3}
250.0	3.33×10^{3}	3.38×10^{3}
300.0	3.64×10^{3}	3.71×10^{3}
350.0	3.94×10^{3}	4.02×10^{3}
400.0	4.28×10^{3}	4.37×10^{3}
500.0	5.01×10^{3}	5.15×10^{3}
600.0	5.68×10^{3}	5.86×10^{3}
700.0	6.25×10^{3}	6.45×10^{3}
800.0	6.72×10^{3}	6.96×10^{3}
900.0	7.12×10^{3}	7.38×10^{3}
1000.0	7.46×10^{3}	7.73×10^{3}

The number of defects has been calculated by the NRT model.

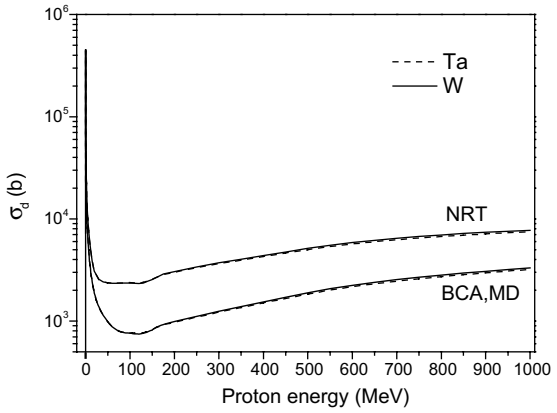

Fig. 8. The total displacement cross-section of tantalum and tungsten obtained with the help of the NRT model and the BCA,MD models. See explanations in the text.

Fig. 9 shows the defect production efficiency η calculated by the discussed combined BCA–MD method for the irradiation of tungsten with As- and W-ions. The efficiency value is shown as a function of the damage energy T_{dam} (Eq. (2)) in the energy range which corresponds to the primary kinetic energy of As- and W-ions up to 1 GeV.

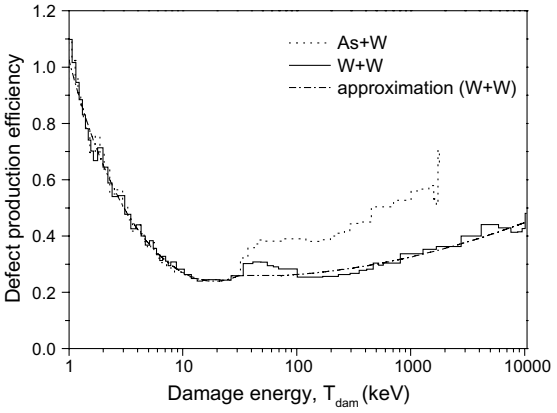

Fig. 9. The efficiency of the defect production in tungsten irradiated with As- and W-ions obtained with the help of the combined BCA–MD method. The approximating curve is shown for W + W irradiation (Eq. (4)).

The defect production efficiency calculated for the W + W irradiation (Fig. 8) can be approximated by the following functions

$1\,\mathrm{keV} \leqslant T_{\mathrm{dam}} \leqslant 31.02\,\mathrm{keV}$ [8]:

$$\eta = 1.0184\,T_{\mathrm{dam}}^{-0.667} + 5.06 \times 10^{-3} T_{\mathrm{dam}}, \quad (4a)$$

$31.02\,\mathrm{keV} < T_{\mathrm{dam}} \leqslant 72.08\,\mathrm{keV}$:

$$\eta = 0.26, \quad (4b)$$

$72.08\,\mathrm{keV} < T_{\mathrm{dam}} \leqslant 10^4\ \mathrm{keV}$:

$$\eta = 5.71 \times 10^{-3} \ln^2(T_{\mathrm{dam}}) - 3.87 \times 10^{-2} \ln(T_{\mathrm{dam}}) \times 10 + 0.32 \quad (4c)$$

It is supposed that the defect production efficiency has a constant value below 1 keV and is equal to $\eta(1\,\mathrm{keV}) = 1.023$.

The combined BCA–MD calculations together with nuclear model calculations were carried out for the irradiation of tungsten with protons at energies up to 1 GeV. The number of defects was calculated as described above.

The recoil characteristics were calculated with the help of the MCNPX code using the Bertini/Dresner model. The simulation of the defect production has been made for each recoil atom with the atomic number $Z > 2$ produced in the p + W interaction with the help of the BCA model and the results of the MD simulation as described above. Table 2 shows the results obtained for the proton irradiation of ^{184}W. Table 2 shows also the nonelastic displacement cross-section calculated using the NRT model and the $\sigma_{\mathrm{d,non}}$ values obtained by the constant approximation of the efficiency η above 31 keV.

In the last case, the $\eta(T)$ value has been calculated using (Eq. (4a)) obtained in Ref. [8]. At energies above 31 keV the constant value equal to 0.26 has been used for the calculations as adopted in the analysis [8] of the high-energy proton irradiation of tungsten. One can see a certain difference between the 'constant approach' and the result of the combined BCA–MD calculations. The most difference is about 60% at the proton energy equal to 1 GeV. Apparently, the increase of the efficiency at the high energies, $T_{\mathrm{dam}} > 70$ keV (Fig. 9) results from the growth of the number of atomic collisions with relatively small energies transferred from the projectile to lattice ions with the increase of the projectile energy. Small energies transferred to PKAs correspond to the region with high values of the defect production efficiency (Fig. 9) and result in the growth of the total efficiency and the displacement cross-section for the projectile comparing with the 'constant efficiency' approach.

The elastic displacement cross-section was calculated as described in Section 1. Eqs. Eqs. (2) and (4) were used for the calculation of the number of defects.

Figs. 8 and 10 show the total displacement cross-section σ_{d} for tungsten calculated using the BCA and MD models. Fig. 10 presents also the σ_{d} values derived from the experimental resistivity damage rates in Ref. [39] and recovered using the Frenkel pair resistivity equal to 27 μΩm for tungsten [6]. The figure shows the data from Ref. [39] which lie between the results obtained with the help of the BCA, MD models and by the NRT approach at the proton energy above 0.2 MeV. The discrepancy between σ_{d} derived from the experiments [39] and the BCA–MD calculations is not yet clear. It can be related to the problem of the initial damage rate measurements and σ_{d} derivation for tungsten or to the problems of the MD simulation in Ref. [8]. The same discrepancy was observed in Ref. [8] for the experimental resistivity change in the high-energy proton irradiation of tungsten and for the results obtained with the help of the MD model.

Table 2
Nonelastic displacement cross-sections for p + ^{184}W interaction calculated with the help of the combined BCA–MD approach (column 2), with the constant approximation of the defect production efficiency value above 31 keV (column 3) and with the help of the NRT model (column 4)

Proton energy (MeV)	Displacement cross-section (b)		
	BCA–MD	MD, above 31 keV η = const	NRT
100	469	517	1987
150	673	643	2474
200	855	754	2901
300	1141	925	3560
400	1468	1111	4275
600	2166	1507	5797
800	2728	1784	6864
1000	3183	1971	7582

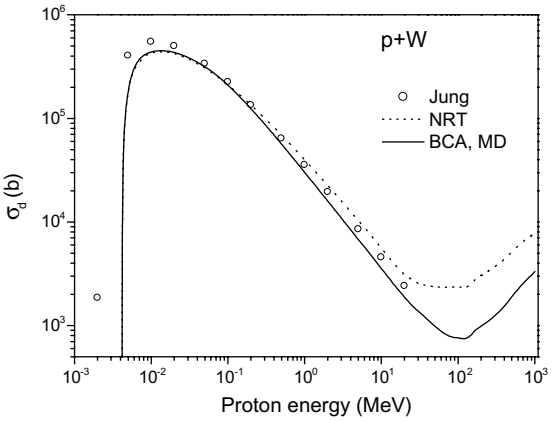

Fig. 10. The total displacement cross-section of tungsten irradiated with protons calculated with the help of the BCA and MD models (solid line), calculated by the NRT model (dashed line) and derived from experimental data in Ref. [39] (cycles).

Table 3
The ratio of the displacement cross-section of tungsten obtained with the help of the BCA and MD models to the cross-sections calculated with the help of the NRT model

Proton energy (MeV)	σ_d (BCA–MD)/σ_d (NRT)
4.1×10^{-3}	1.023
5.5×10^{-2}	1.023
9.7×10^{-2}	0.993
0.13	0.965
0.16	0.942
0.20	0.917
0.25	0.892
0.31	0.869
0.39	0.844
0.49	0.821
0.63	0.796
0.81	0.773
1.0	0.755
1.3	0.735
1.7	0.716
2.4	0.695
3.5	0.675
5.0	0.658
10.0	0.634
15.0	0.628
20.0	0.611
25.0	0.578
30.0	0.540
35.0	0.507
40.0	0.472
45.0	0.442
50.0	0.414
60.0	0.378
70.0	0.350
80.0	0.333
100.0	0.322
200.0	0.324
300.0	0.336
400.0	0.352
500.0	0.367
600.0	0.382
700.0	0.393
800.0	0.405
900.0	0.416
1000.0	0.427

Table 3 shows the ratio of the displacement cross-section obtained by the BCA and MD models to the σ_d cross-section calculated with the help of the NRT model (Table 1).

3.2. Tantalum

There is no detailed information about the energy dependence of the defect production efficiency η for tantalum. The comparison of the averaged efficiency values derived from the neutron irradiation experiments [6] shows that the $\langle\eta\rangle$ values for tantalum and tungsten are very close. Moreover, both metals have a bcc lattice, the same effective threshold displacement energy and similar nuclear properties. This justifies the use of the main results obtained for tungsten in the present work (Section 3.1) for the approximate data evaluation for tantalum.

The ratio of the displacement cross-section calculated using the BCA and MD models for the σ_d value obtained by the NRT approach shown in Table 3 for tungsten, is the average defect production efficiency $\langle\eta\rangle$ related to a certain initial proton energy. These $\langle\eta\rangle$ values can be used with some reservation obtaining the approximate displacement cross-section for tantalum basing on the σ_d values presented in Table 1. These evaluated values are presented in Fig. 8.

One should note that the uncertainty in the σ_d values obtained using different nuclear models (Section 2.2) is more than the expected difference between realistic displacement cross-sections for tantalum and tungsten. This conclusion results from the similar $\langle\eta\rangle$ values for tantalum and tungsten obtained from the analysis of measured resistivity damage rates in various neutron irradiation experiments ($\langle\eta\rangle$(Ta) = 0.73 ± 0.09, $\langle\eta\rangle$(W) = 0.61 ± 0.08). It cannot diminish the importance of the further investigations for tantalum.

4. Conclusion

The displacement cross-section has been calculated for tantalum and tungsten irradiated with protons at energies from several keV up to 1 GeV using the different nuclear models and approaches to obtain the number of defects in irradiated material.

The displacement cross-section for proton elastic scattering $\sigma_{d,el}$ has been calculated using the data from ENDF/B-VI Proton Sublibrary (Release 7) and with the help of the optical model. The good agreement was found between the $\sigma_{d,el}$ values obtained using various modern optical potentials. The displacement cross-section for the proton nonelastic interactions $\sigma_{d,non}$ has been calculated with the help of the different nuclear models incorporated in the MCNPX code [9]. The satisfactory agreement is observed for the $\sigma_{d,non}$ values obtained using the ENDF/B-VI data for tungsten and the calculations by the Bertini/Dresner model and the ISABEL/Dresner model. The total displacement cross-section has been evaluated for tantalum and tungsten at energies from the several keV up to 1 GeV. The results obtained with the help of the NRT model is shown in Table 1.

The number of defects produced under the high energy proton irradiation of tungsten was calculated with the help of the BCA model [38] using the results of the MD simulation [8]. The realistic displacement cross-section and the defect production efficiency have been obtained for tungsten at proton energies up to 1 GeV

(Figs. 8 and 10, Tables 2 and 3). The approximate σ_d values for tantalum are shown in Fig. 8.

A further theoretical and experimental study is necessary to obtain the realistic displacement cross-sections for tantalum. The measurements should be carried out for the resistivity damage rates in tantalum and tungsten irradiated with the particles of various energies to get the information about the energy dependence of the number of defects produced. This could give an answer together with a new measurement of the Frenkel pair resistivity about the discrepancy of the experimental damage characteristics and the results of calculations performed in the present work and in Ref. [8].

References

[1] TRADE Final Feasibility Report – March 2002 by the Working Group on TRADE: TRiga Aceelerator Driven Experiment (2002).
[2] M.W. Guinan, J.H. Kinney, J. Nucl. Mater. 108&109 (1982) 95.
[3] C.E. Klabunde, R.R. Coltman, J. Nucl. Mater. 108&109 (1982) 183.
[4] S. Takamura, T. Aruga, K. Nakata, J. Nucl. Mater. 136 (1985) 159.
[5] G. Wallner, M.S. Anand, L.R. Greenwood, M.A. Kirk, W. Mansel, W. Waschkowski, J. Nucl. Mater. 152 (1988) 146.
[6] C.H.M. Broeders, A.Yu. Konobeyev, J. Nucl. Mater. 328 (2004) 197.
[7] M.J. Norgett, M.T. Robinson, I.M. Torrens, Nucl. Eng. Des. 33 (1975) 50.
[8] M.J. Caturla, T. Diaz de la Rubia, M. Victoria, R.K. Corzine, M.R. James, G.A. Greene, J. Nucl. Mater. 296 (2001) 90.
[9] J.S. Hendricks, G.W. McKinney, L.S. Waters, T.L. Roberts et al., MCNPX, Version 2.5.d, Report LA-UR-03-5916 (2003).
[10] M.T. Robinson, J. Nucl. Mater. 216 (1994) 1.
[11] J. Lindhard, M. Scharff, H.E. Schiott, K. Dan. Vidensk. Selsk. Mat. Fys. Medd. 33 (14) (1963) 1.
[12] K.B. Winterbon, P. Sigmund, J.B.K. Sanders, K. Dan. Vidensk. Selsk. Mat. Fys. Medd. 37 (14) (1970) 1.
[13] P. Schwandt, H.O. Meyer, W.W. Jacobs, A.D. Bacher, S.E. Vigdor, M.D. Kaitchuck, et al., Phys. Rev. C 26 (1982) 55.
[14] R.L. Walter, P.P. Guss, Radiat. Eff. 92 (1985) 1079.
[15] D.G. Madland, OECD/NEA Spec. Mtg. Nucleon-Nucleus Opt. Mod. to 200 MeV, Paris, 1997, p. 129.
[16] A.J. Koning, J.P. Delaroche, Nucl. Phys. A 713 (2003) 231.
[17] H. Kamitsubo, H. Ohnuma, K. Ono, A. Uchida, M. Imaizumi, S. Kobayashi, M. Sekiguchi, J. Phys. Soc. Jpn. 22 (1967) 19.
[18] D.J. Steinberg, J.N. Palmieri, A.M. Cormack, Nucl. Phys. 56 (1964) 46.
[19] R.E. Richardson, W.P. Ball, C.E. Leith, B.J. Moyer, Phys. Rev. 86 (1952) 29.
[20] L.S. Waters (Ed.), MCNPX™ User's manual, Version 2.3.0, LA-UR-02-2607 (2002).
[21] H.W. Bertini, Phys. Rev. 131 (1963) 1801.
[22] H.W. Bertini, Phys. Rev. 188 (1969) 1711.
[23] L. Dresner, Report ORNL-TM-196 (1962).
[24] K. Chen, Z. Fraenkel, G. Friedlander, J.R. Grover, J.M. Miller, Y. Shimamoto, Phys. Rev. 166 (1968) 949.
[25] Y. Yariv, Z. Fraenkel, Phys. Rev. C 20 (1979) 2227.
[26] Y. Yariv, Z. Fraenkel, Phys. Rev. C 24 (1981) 488.
[27] A.S. Iljinov, JINR Report B1-4-5478, Dubna (1970).
[28] V.S. Barashenkov, V.D. Toneev, Interaction of High Energy Particles and Nuclei with Atomic Nuclei, Atomizdat, Moscow, 1972.
[29] K.K. Gudima, S.G. Mashnik, V.D. Toneev, Nucl. Phys. A 401 (1983) 329.
[30] S.G. Mashnik, Nucl. Phys. A 568 (1994) 703.
[31] S.G. Mashnik, R.J. Peterson, A.J. Sierk, M.R. Braunstein, Phys. Rev. C 61 (2000) 034601.
[32] J. Cugnon, C. Volant, S. Vuillier, Nucl. Phys. A 620 (1997) 475.
[33] A. Boudard, J. Cugnon, S. Leray, C. Volant, Phys. Rev. C 66 (2002) 044615.
[34] K.-H. Schmidt, M.V. Ricciardi, A.S. Botvina, T. Enqvist, Nucl. Phys. A 710 (2002) 157.
[35] K.-H. Schmidt, J. Benlliure, A.R. Junghans, Nucl. Phys. A 693 (2001) 169.
[36] W.A. Richter, S.W. Steyn, A.A. Cowley, J.A. Stander, J.W. Koen, R. Lindsay, G.C. Hillhouse, R.E. Julies, J.J. Lawrie, J.V. Pilcher, P.E. Hodgson, Phys. Rev. C 54 (1996) 1756.
[37] M.W. Guinan, J.H. Kinney, J. Nucl. Mater. 103&104 (1981) 1319.
[38] C.H.M. Broeders, A.Yu. Konobeyev, K. Voukelatou, IOTA – a Code to Study Ion Transport and Radiation Damage in Composite Materials, Forschungszentrum Karlsruhe Report, FZKA 6984, August 2004.
[39] P. Jung, J. Nucl. Mater. 117 (1983) 70.
[40] M.S. Wechsler, C. Lin, W.F. Sommer, L.L. Daemon, P.D. Ferguson, J. Nucl. Mater. 244 (1997) 177.
[41] M.H. Barnett, M.S. Wechsler, D.J. Dudziak, R.K. Corzine, L.A. Charlton, L.K. Mansur, in: Proceedings of the Third International Topical Meeting on Nuclear Applications of Accelerator Technology, LaGrande Park, Illinois, 1999, p. 555.
[42] I. Jun, IEEE Trans. Nucl. Sci. 48 (2001) 162.